

Kinetics of the iron α - ε phase transition at high-strain rates: Experiment and modelN. Amadou,^{1,2,3,*} T. de Resseguier,² E. Brambrink,¹ T. Vinci,¹ A. Benuzzi-Mounaix,¹ G. Huser,⁴ G. Morard,⁵ F. Guyot,⁵ K. Miyanishi,⁶ N. Ozaki,^{6,7} R. Kodama,^{6,7} and M. Koenig^{1,8}¹LULI-CNRS, Ecole Polytechnique, CEA: Université Paris-Saclay; UPMC Université Paris 06: Sorbonne Universités, F-91128 Palaiseau Cedex, France²Institut Pprime, CNRS, ENSMA, Université de Poitiers, F-86000 Poitiers, France³Département de Physique, Université Abdou Moumouni de Niamey, BP. 10662 Niamey, Niger⁴CEA, DAM, DIF, F-91297 Arpaçon, France⁵Institut de Minéralogie, de Physique des Matériaux et Cosmochimie (IMPMC), MNHN, CNRS, UPMC, IRD, Sorbonne Universités, F-75005 Paris, France⁶Graduate School of Engineering, Osaka University, Suita, Osaka 565-0871, Japan⁷Photon Pioneers Center, Osaka University, Suita, Osaka 565-0871, Japan⁸Institute for Academic Initiatives, Osaka University, Suita, Osaka 565-0871, Japan

(Received 27 January 2016; revised manuscript received 22 April 2016; published 14 June 2016)

In this article, we investigate the kinetics of the iron α - ε transition under laser-driven ramp compression for deformation rates ranging from 3 to 9×10^7 s⁻¹. As in previous work, we observe a plateau in the rear surface velocity profile at the transition. With increasing deformation rate the transition onset pressure raises from 11 to 25 GPa, while the plateau duration decreases. These kinetic effects are well reproduced by an Avrami-type kinetics model of nucleation and growth with a constant, nanosecond scale completion time, which suggests an isokinetic regime over the explored range of strain rates.

DOI: [10.1103/PhysRevB.93.214108](https://doi.org/10.1103/PhysRevB.93.214108)**I. INTRODUCTION**

Solid-solid polymorphic phase transitions under dynamic compression play key roles for (i) material science where they offer ways to synthesize materials for technological applications [1,2]; (ii) planetary science (including geophysics) where they are fundamental for understanding Earth and telluric exoplanet internal structure [3–5]; and (iii) condensed matter physics, where they give insight into atomic rearrangement under extreme conditions [6–9]. In particular, laser-driven compression experiments can provide insight into some specific features of phase transformation such as new phase nucleation and growth rates, the transition characteristic time, the transition stress and compression, etc. [6,10,11].

The most famous and widely studied example of such solid-solid phase transition is the martensitic transformation of iron from the ground state body-centered cubic (bcc) structure (α phase) to the high pressure hexagonal close-packed (hcp) structure (ε phase) around a pressure of 13 GPa. Since its discovery by Bancroft *et al.* in 1956 [12], this transition has been extensively studied under both static [9] and standard shock compression [6,10,13–15].

Recently, efforts have been focused on investigating the phase transition kinetics and dynamical behavior using ramp compression which gives a continuous information along the compression path. Fast compressed diamond anvil cells have provided *in situ* data on the progress of the transition at low strain rates in the $10^{-2} - 10^2$ s⁻¹ range [16]. At much higher rates, Bastea *et al.* [17] have reported Z-pinch quasi-isentropic compression of iron, for thick targets (≈ 500 μ m) and long compression times (≈ 200 ns), where transition kinetics has been explored by varying the target initial temperature. By

using a phase nucleation and growth kinetic model with pressure dependent phase interface velocity, they found that the thermodynamic path followed by the sample is strongly dependent on the drive conditions and probably on the target characteristics.

In a previous article, we have reported on the kinetic effects of the iron α - ε transition under different laser ramp loading conditions [18] where it was shown that the transition leads to a plateau in the VISAR measured velocity profile. Upon increasing the loading rate, this plateau is shifted to higher velocities while its duration decreases. In a subsequent article by Smith *et al.* [11], a time-dependence study of the α - ε phase transformation under wide experimental conditions (compression time between 3 and 300 ns and sample thickness from 10 μ m up to millimeter) was reported. One pointing out of this latter work was that treating the kinetics of the phase transformation locally as a function of the difference in free energy with a constant time scale for the transition reproduces quite poorly the velocity histories which suggests the need for more explicit representation of the nucleation of daughter phase within the parent followed by growth from the nuclei to capture the response of the material under highly dynamic deformation. Here, we report on a complementary experimental and numerical investigation of the iron α - ε dynamical phase transition kinematics under different laser ramp compression loading conditions. The deformation rates range from $\dot{\varepsilon} = 3.2$ to 8.6×10^7 s⁻¹. Over this relatively narrow range it is found that an Avrami-type transition model based on a theoretical description of nucleation and growth mechanism reproduces well the measured velocity profiles with a constant characteristic time, which indicates an isokinetic regime in which the transformation kinetics remains invariant.

The article layout is as follows: In Sec. II we describe the experiment setup and results while in Sec. III we present

*nourou.amadou@polytechnique.edu

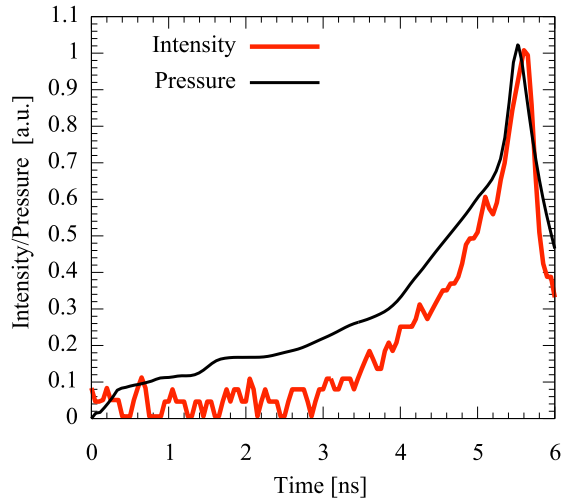


FIG. 1. Optimized laser pulse (red thick curve) used during our experience and the resulting pressure loading profile (black thin curve) at the target front surface as simulated by the code MULTI [19].

the phase transition kinetics model. The results are discussed in Sec. IV and finally the main conclusions are presented in Sec. V.

II. EXPERIMENT AND RESULTS

The experiment was performed at the LULI2000 laser facility where a 5-ns laser pulse with energy up to 250 J at 532 nm was used to drive a ramp compression into thin polycrystalline iron target. To ensure a uniform compression front, a hybrid phase plate (HPP) was used to obtain a smooth flat profile with 800 μm diameter. Temporal laser pulse shaping was used to optimize the ramp profile using a model based on [20,21] resulting in an exponential type laser profile, as shown in Fig. 1.

The target was a 9.5- μm thick iron sample either freestanding or attached on a 1-mm thick sapphire window. Direct, high intensity laser irradiation of mid-Z elements can generate suprathermal electrons and/or x rays which may preheat the sample ahead of the compression wave. According to computations of laser-matter interaction described in Sec. III, where thermal radiation transport and heat conduction are accounted for, the maximum electronic temperature in our shot conditions is about 800 eV for a very short time at the end of the laser pulse. The penetration depth in iron of the relatively soft x rays produced at such moderate temperature is in the order of 1 μm , so that preheating will not affect wave propagation and subsequent phase transformation throughout our 9.5- μm thick sample.

When the compression wave breaks out, the target rear surface expands into the vacuum or into the sapphire window. The temporal profile of the rear surface velocity was measured using two-channel velocity interferometer system for any reflector (VISAR) [22], with temporal and spatial resolutions of 100 ps and 10 μm , respectively. An example of raw VISAR record is shown in Fig. 2 (bottom) with the resulting rear surface velocity temporal profile (top).

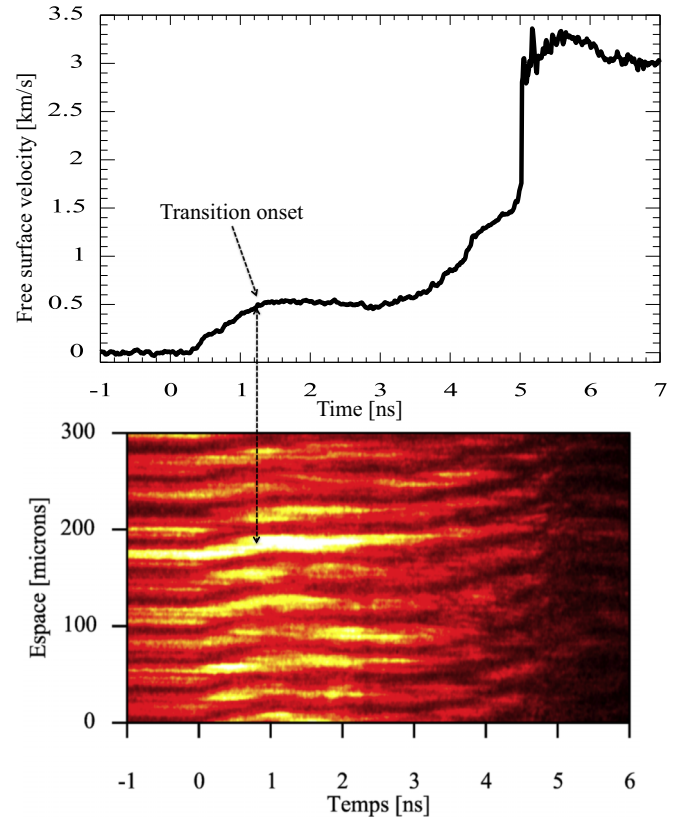


FIG. 2. An example of raw VISAR recorded data (bottom) with the resulting rear surface velocity temporal profile (top). The iron α - ε transition results in a plateau at 0.56 km/s in the profile.

The data shown in Fig. 2 corresponds to the shot of lowest peak intensity ($3.7 \times 10^{12} \text{ W/cm}^2$). The plateau at the free surface velocity of 0.56 km/s is due to the iron α - ε phase transformation. The iron elastic-plastic transition is expected to produce a small step precursor at about 100 m/s, which is not observed, probably due to the small thickness of our target [6].

In order to investigate the iron α - ε transition dynamics under ramp compression, the laser peak intensity was varied from $3.7 \times 10^{12} \text{ W/cm}^2$ to $16 \times 10^{12} \text{ W/cm}^2$ (increasing the laser energy while keeping the temporal profile of the laser pulse fixed). The corresponding mean deformation rates, inferred from simulations described in Sec. III range from $3.2 \times 10^7 \text{ s}^{-1}$ for the laser intensity of $3.7 \times 10^{12} \text{ W/cm}^2$ to $8.6 \times 10^7 \text{ s}^{-1}$ for the laser intensity of $16 \times 10^{12} \text{ W/cm}^2$. Under such increasing strain rate the particle velocity where the transition occurs increases while the plateau duration decreases (see Fig. 3). This behavior is the direct consequence of the phase transition kinetic effects and is comparable to that reported recently on iron α - ε transition under ramp compression [11]. To simulate experiments the kinetics of the phase transition have to be taken into account as shown in the following section.

III. NUMERICAL SIMULATIONS

For each shot, a first simulation of laser-matter interaction is performed with the 1D hydrodynamic code MULTI [19],

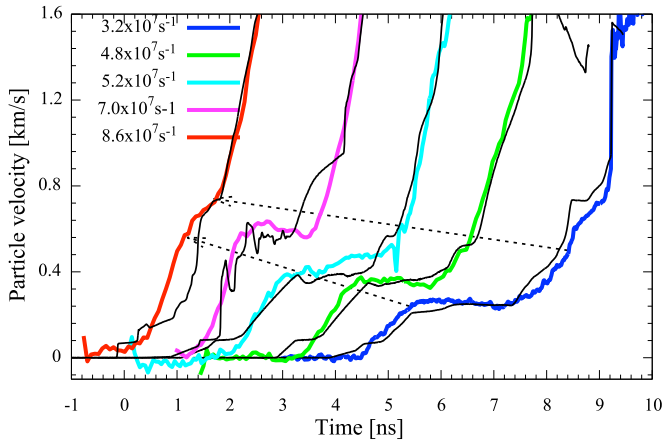


FIG. 3. VISAR profiles for different lasers intensities (thin black lines are numerical simulations). The onset velocity of the iron α - ε transition increases with the increase of the laser intensity while the plateau duration decreases. The particle velocity was obtained from the rear surface velocity by applying the sapphire refractive-index correction in the case of Fe/sapphire target [15,23,24] and by supposing a good impedance matching between the iron and sapphire [17] (shot $4.8 \times 10^7 \text{ s}^{-1}$, $5.2 \times 10^7 \text{ s}^{-1}$, and $7 \times 10^7 \text{ s}^{-1}$) or applying standard $2u_p = u_f$ formula for free standing target [11] (shot $3.2 \times 10^7 \text{ s}^{-1}$ and $8 \times 10^7 \text{ s}^{-1}$). For better readability, the velocity profiles are temporally shifted.

using the measured profile of laser intensity as input boundary condition and material data from the SESAME tables. As mentioned above, it shows that radiative preheating from the plasma is not significant in the probed region. Thus, the difference between the temperature computed in this region with or without radiation transport is less than 50 K for compression below 100 GPa, where phase transformation is investigated. This simulation provides the amplitude and temporal shape of the pressure ramp induced beneath the irradiated surface (see Fig. 1). Then, this calculated ramp profile is used as a boundary condition in the 1D hydrodynamic code SHYLAC [25,26] to simulate the dynamic response of iron, including the kinetics of the phase transition. Each cell is considered as a mixture of α and ε phases (subscripts 1 and 2, respectively). X is defined as the mass fraction of the ε phase ($0 < X < 1$). The specific volume V and specific internal energy E of the mixture are expressed in terms of the specific volumes V_1 , V_2 and specific internal energies E_1 , E_2 of the pure-phase constituents:

$$V = (1 - X)V_1 + XV_2, \quad (3.1)$$

$$E = (1 - X)E_1 + XE_2. \quad (3.2)$$

As in previous work on phase transformation, pressure, and thermal equilibrium is assumed between the two phases:

$$P(E, V) = P_1(E_1, V_1) = P_2(E_2, V_2), \quad (3.3)$$

$$T(E, V) = T_1(E_1, V_1) = T_2(E_2, V_2), \quad (3.4)$$

with the details of the equation of state for each pure phase described in Refs. [25,26]. The evolution of the epsilon mass

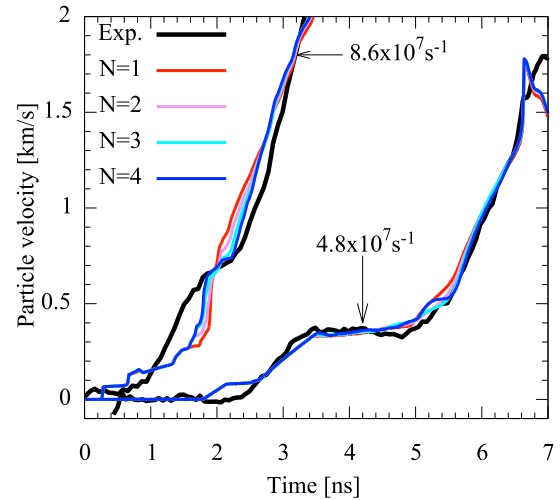


FIG. 4. Influence of the N parameter on the transition kinetics for $\theta = 1 \text{ ns}$ and $\dot{\varepsilon}$ equals $4.8 \times 10^7 \text{ s}^{-1}$ and $8.6 \times 10^7 \text{ s}^{-1}$.

fraction X is governed by a kinetics law derived as follows. As an epsilon nucleon grows with the speed u , the size of the nucleon at time t is given by

$$v(t) = D(ut)^d, \quad (3.5)$$

where $d = 1, 2, 3$ represent the dimension (linear, planar or spherical) of the growth of the epsilon phase and D is a shape factor equal to $2, \pi, 4\pi/3$ for $d = 1, 2, 3$, respectively. The epsilon mass fraction, according to the kinetics theory of Avrami [27–29], is thus given by

$$X(t) = 1 - \exp\left(-R \int_0^t v(t') dt'\right), \quad (3.6)$$

with R , the nucleation rate. Replacing $v(t)$ by Eq. (3.5) and integrating, it comes that

$$X(t) = 1 - \exp\left[-\frac{D}{N} \left(\frac{t}{\theta}\right)^N\right], \quad (3.7)$$

with $N = d + 1$ and $\theta = (Ru^d)^{-1/N}$. θ is thus a characteristic time that can be seen as the completion time for the phase transformation. In practice, the phase transformation starts where and when the Gibbs free energy of the epsilon phase becomes less than the alpha phase one, then its evolution is governed by Eq. (3.7). N and θ are the only two free parameters of the model. In a first, simple attempt to test the model, they are fixed at constant values, which will be discussed in details in the next section.

From the compression volume profile $V(t)$ computed near the ramp-loaded surface, a mean strain rate $\dot{\varepsilon} = \frac{1}{V_0} \frac{dV}{dt}$, with V_0 the initial volume, was calculated for each shot. For lower deformation rate ($\dot{\varepsilon} < 7 \times 10^7 \text{ s}^{-1}$), the simulations are less sensitive to N . For ($\dot{\varepsilon} > 7 \times 10^7 \text{ s}^{-1}$) the best match between experiment and simulations was found for $N = 4$, equivalently $d = 3$ (see Fig. 4). Thus, we conclude that growth process is three-dimensional. Concerning the influence of the characteristic time θ , we have found that the larger θ the stiffer the slope of transition plateau while the plateau duration remains roughly the same (see Fig. 5). For all our shots, the best

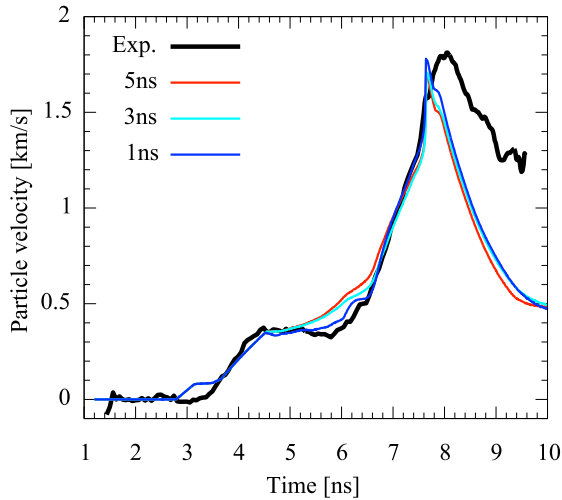


FIG. 5. Influence of the characteristic time θ on the velocity profile for $N = 4$ and $\dot{\epsilon} = 4.8 \times 10^7 \text{ s}^{-1}$.

agreement between experiments and simulations was obtained for $\theta = 1 \text{ ns}$ (see thin black curves on Fig. 3).

It is also worth noting that this Avrami-based model agrees better with experiment than the Hayes empirical kinetics model [30] which was used in earlier works [25,26]. Indeed, there is no characteristic time for which the Hayes model can reproduce correctly the experimental results at higher strain rates, including the observed plateau (see Fig. 6). This corroborates the statement that a model which treats the kinetics of the phase transformation only as a function of the difference in free energy should not reproduce the velocity profile for high deformation rate as reported in Ref. [11].

IV. DISCUSSION

To investigate the coupling between compression dynamics and transition kinetics, the propagation distance from the

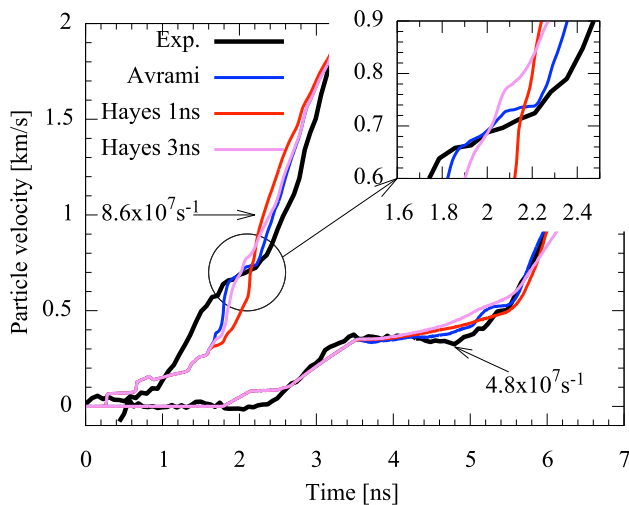


FIG. 6. Comparison between Avrami and Hayes model for $\dot{\epsilon}$ equals $4.8 \times 10^7 \text{ s}^{-1}$ and $8.6 \times 10^7 \text{ s}^{-1}$. The Avrami simulations were done with $N = 4$ and $\theta = 1 \text{ ns}$. The inset is a zoom on the high deformation rate ($8.6 \times 10^7 \text{ s}^{-1}$) phase transition region.

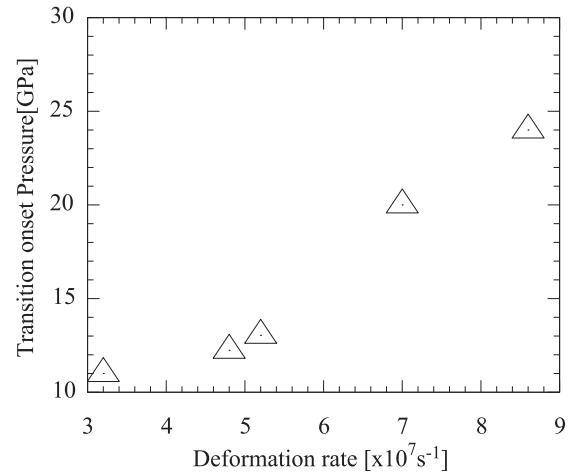


FIG. 7. The transition onset pressure for different deformation rate.

loaded surface to the probed surface (target thickness) is crucial. A sufficient propagation distance is necessary to start forming the plateau, as it is the result of the sound speed change at the phase transition. However, progressive wave separation leads to a local decrease of the strain rate at the plateau pressure, which in turn will lower the transition onset during propagation. This process will continue until reaching a stationary regime over larger propagation distance, where the wavefront is no longer affected by transient kinetic effects. Therefore, the small thickness of our targets ($9.5 \mu\text{m}$) is an important precondition to observe such kinetic effects in the velocity profiles.

As stated in Sec. III, the phase transformation is initiated when the Gibbs free energy of the epsilon phase becomes lower than that of the alpha phase. Thus, this thermodynamic initiation is not strain rate dependent. However, because subsequent growth of the epsilon phase is limited by its kinetics, its proportion remains very small for a short time (that can be seen as an incubation time) during which the macroscopic behavior of the mixture is still essentially that of alpha-iron. The velocity plateau starts only after this delay, once the amount of epsilon phase becomes sufficient to affect wave propagation. To present our results in similar terms as in previous work [11,17], we associate this threshold, significant amount of epsilon phase to the “onset” of the transformation. Because the thermodynamic conditions evolve before reaching this stage, the onset pressure is strain-rate dependent. It is inferred at each shot from the velocity value at the measured plateau, and plotted versus strain rate in Fig. 7. It is found to vary from 11 GPa for $\dot{\epsilon} = 3.2 \times 10^7 \text{ s}^{-1}$ to 25 GPa for $\dot{\epsilon} = 8.6 \times 10^7 \text{ s}^{-1}$ (Fig. 7). The transformation onset pressure for the smallest deformation rate is below the equilibrium value of 13 GPa. This may be due to the presence of large defect density in a thinner target which should lower the transition threshold by locally reducing the Gibbs free energy barrier between both phases and thus lowering down the transition onset pressure [7,8].

At higher rates, pressure overshoot conforms to that reported previously under ramp compression [11]. However, the Avrami-based approach adopted here differs substantially

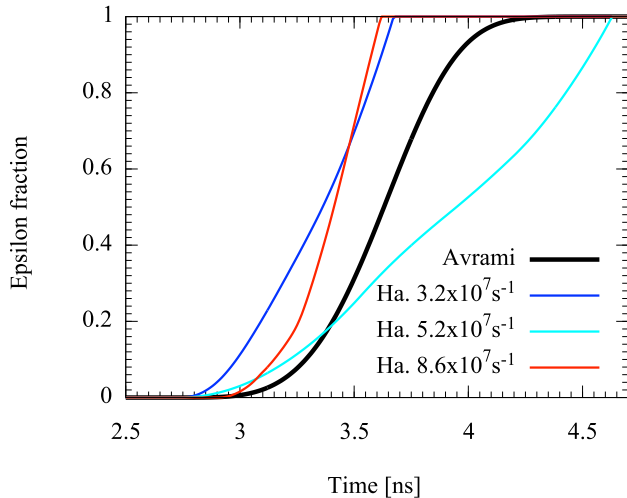


FIG. 8. Computed evolution of the epsilon fraction during the phase transformation under different loading rates (see Fig. 3), with a 1-ns characteristic time. In the Avrami model (thick black line), the temporal evolutions is the same for all shots, with a characteristic sigmoidal shape, while in the Hayes model (thin lines), the strain rate directly affects the transformation duration.

from the kinetics model in [11], where an explicit dependence of the transition rate on over-pressurization was introduced in the form of a three-stage function fitted empirically. Instead, we consider a simple, intrinsic transformation behavior involving one geometrical parameter N and one characteristic time θ combining both nucleation (through R) and growth (through u) of the daughter phase. Physically, the correct match for $N=4$ suggests 3D spherical growth of the nuclei. Because this shape allows minimizing the interface energy between both phases, it indicates that the contribution of this interface energy is important in the transition energetics [8]. This N value of 4 has been reported to match a number of polymorphic transformations with nucleation at constant or increasing rate [31]. The use of a constant θ value corresponds to a regime referred to as isokinetic, where the transition kinetics is independent of the strain rate, like evidenced originally by Avrami as some range of temperatures and concentrations in which the characteristic kinetics of phase change remains unchanged [27]. Thus, the computed variations of the ϵ fraction are identical for all shots, with a sigmoidal shape (Fig. 8). This shape was acknowledged as a general requirement for quantitative description of the kinetics of many types of phase transformations [27]. It was later reported as a nearly universal shape of growth curves for first-order phase transformations under quasistatic compression at room temperature [32]. Our results suggest that this shape is important to capture the behavior observed at very high-strain rates, which the Hayes model fails to reconstitute, as mentioned in Sec. III. The 1-ns value of the transition time is consistent with a previous report

under laser shock compression where the characteristic time was found to be 2–5 ns [10,25,26].

However, in the literature it seems that this value should vary with the deformation rate [17,32]. The isokinetic regime (i.e., the fact that a single characteristic time θ fits all deformation rates) evidenced in our experiments is probably due to the narrow explored range ($3-9 \times 10^7 \text{ s}^{-1}$). Over this range, the observed influence of the strain rate, although of obvious importance, is thus not directly dominated by the transformation kinetics itself but rather by the evolution of the thermodynamic conditions during the transformation, with an interplay between sound velocity increase with pressure and sound velocity decrease upon phase transition. In particular, the variations of onset pressure are governed by the maximum compression reached during the early stage of slow transformation, then the sharp growth of ϵ proportion induces a fast decrease of the sound speed which leads to the pronounced plateau in the velocity profiles. Nevertheless, it is not excluded that, over larger range of deformation rates or various target thickness and preparation conditions as reported in Ref. [11], the isokinetic assumption should be revised and the characteristic time should be modified.

V. CONCLUSIONS

We have investigated the dynamics of the iron α - ϵ transition under ramp compression for different deformation rates ranging from 3 to $9 \times 10^7 \text{ s}^{-1}$. As in previous work, we have observed a plateau in the rear surface velocity profile at the transition. The higher the deformation rate the higher the transition onset pressure and the smaller the plateau duration. We have shown that behavior is well reproduced by an Avrami-type kinetics model with a constant characteristic time. This implies an isokinetic regime in which the characteristic kinetics of the phase change is independent on the strain rate. Thus, the observed effects are dominated by the thermomechanical response and wave propagation during the phase transformation rather than by the kinetics of this transformation. The 1-ns value of the characteristic time is consistent with that reported for this transition under laser shock compression.

ACKNOWLEDGMENTS

We thank the crew of the LULI2000 laser facility for their ongoing support during the experiment. This work was supported in part by JSPS KAKENHI (Grant No. 22224012), JSPS core-to-core program on International Alliance for Material Science in Extreme States with High Power Laser and XFEL, and the X-ray Free Electron Laser Priority Strategy Program at Osaka University from the Ministry of Education, Culture, Sports, Science and Technology (MEXT) and the french ANR program SECHEL.

- [1] P. S. DeCarli and J. C. Jamieson, Formation of diamond by explosive shock, *Science* **133**, 1821 (1961).
 [2] D. J. Milton and P. S. de Carli, Maskelynite: Formation by explosive shock, *Science* **140**, 670 (1963).

- [3] R. L. Kovach and D. L. Anderson, The interiors of the terrestrial planets, *J. Geophys. Res.* **70**, 2873 (1965).
 [4] D. Valencia *et al.*, Internal structure of massive terrestrial planets, *Icarus* **181**, 545 (2006).

- [5] C. Sotin, Mass-radius curve for extrasolar Earth-like planets and ocean planets, *Icarus* **191**, 337 (2007).
- [6] J. Hawreliak, J. D. Colvin, J. H. Eggert, D. H. Kalantar, H. E. Lorenzana, J. S. Stölken, H. M. Davies, T. C. Germann, B. L. Holian, K. Kadau, P. S. Lomdahl, A. Higginbotham, K. Rosolankova, J. Sheppard, and J. S. Wark, Analysis of the x-ray diffraction signal for the α - ϵ transition in shock-compressed iron: Simulation and experiment, *Phys. Rev. B*, **74**, 184107 (2006).
- [7] K. Kadau *et al.*, Microscopic view of structural phase transitions induced by shock waves, *Science* **296**, 1681 (2002).
- [8] K. Kadau, T. C. Germann, P. S. Lomdahl, and B. L. Holian, Atomistic simulations of shock-induced transformations and their orientation dependence in bcc Fe single crystals, *Phys. Rev. B* **72**, 064120 (2005).
- [9] F. M. Wang and R. Ingalls, Iron bcc-hcp transition: Local structure from x-ray-absorption fine structure, *Phys. Rev. B* **57**, 5647 (1998).
- [10] D. H. Kalantar, J. F. Belak, G. W. Collins, J. D. Colvin, H. M. Davies, J. H. Eggert, T. C. Germann, J. Hawreliak, B. L. Holian, K. Kadau, P. S. Lomdahl, H. E. Lorenzana, M. A. Meyers, K. Rosolankova, M. S. Schneider, J. Sheppard, J. S. Stölken, and J. S. Wark, Direct Observation of the α - ϵ Transition in Shock-Compressed Iron Via Nanosecond X-Ray Diffraction, *Phys. Rev. Lett.* **95**, 075502 (2005).
- [11] R. F. Smith, J. H. Eggert, D. C. Swift, J. Wang, T. S. Duffy, D. G. Braun, R. E. Rudd, D. B. Reisman, J.-P. Davis, M. D. Knudson, and G. W. Collins, Time dependence of the alpha to epsilon phase transformation in iron, *J. Appl. Phys.* **114**, 223507 (2013).
- [12] D. Bancroft, Eric L. Peterson, and S. Minshall, Polymorphism of iron at high pressure, *J. Appl. Phys.* **27**, 291 (1956).
- [13] L. M. Barker and R. E. Hollenbach, Shock wave study of the α - ϵ phase transition in iron, *J. Appl. Phys.* **45**, 4872 (1974).
- [14] J. C. Boettger and D. C. Wallace, Metastability and dynamics of the shock-induced phase transition in iron, *Phys. Rev. B* **55**, 2840 (1997).
- [15] B. J. Jensen *et al.*, Accuracy limits and window corrections for photon doppler velocimetry, *J. Appl. Phys.* **101**, 013523 (2007).
- [16] Z. Konôpková, A. Rothkirch, A. K. Singh, S. Speziale, and H.-P. Liermann, *In situ* x-ray diffraction of fast compressed iron: Analysis of strains and stress under non-hydrostatic pressure, *Phys. Rev. B* **91**, 144101 (2015).
- [17] M. Bastea *et al.*, High pressure phase transformation in iron under fast compression, *Appl. Phys. Lett.* **95**, 241911 (2009).
- [18] N. Amadou, E. Brambrink, A. Benuzzi-Mounaix, G. Huser, F. Guyot, S. Mazevet, G. Morard, T. de Resseguier, T. Vinci, K. Myanishi, N. Ozaki, R. Kodama, T. Boehly, O. Henry, D. Raffestin, and M. Koenig, Direct laser-driven ramp compression studies of iron: A first step toward the reproduction of planetary core conditions, *High Energy Density Physics* **9**, 243 (2013).
- [19] R. Ramis *et al.*, Multi—a computer code for one-dimensional multigroup radiation hydrodynamics, *Comput. Phys. Commun.* **49**, 475 (1988).
- [20] E. Brambrink, N. Amadou, A. Benuzzi-Mounaix, M. Geissel, M. Harmand, A. Pelka, T. Vinci, and M. Koenig, Production and diagnostics of dense matter, *Contrib. Plasma Phys.* **55**, 67 (2015).
- [21] D. C. Swift, R. G. Kraus, E. N. Loomis, D. G. Hicks, J. M. McNaney, and R. P. Johnson, Shock formation and the ideal shape of ramp compression waves, *Phys. Rev. E* **78**, 066115 (2008).
- [22] L. M. Barker *et al.*, Shock wave studies of PMMA, fused silica, and sapphire, *J. Appl. Phys.* **41**, 4208 (1970).
- [23] D. Hayes, Unsteady compression waves in interferometer windows, *J. Appl. Phys.* **89**, 6484 (2001).
- [24] R. E. Setchell, Refractive index of sapphire at 532 nm under shock compression and release, *J. Appl. Phys.* **91**, 2833 (2002).
- [25] T. de Resseguier and M. Hallouin, Interaction of two laser shocks inside iron samples, *J. Appl. Phys.* **90**, 4377 (2001).
- [26] T. de Resseguier and M. Hallouin, Effects of the α - ϵ phase transition on wave propagation and spallation in laser shock-loaded iron, *Phys. Rev. B* **77**, 174107 (2008).
- [27] M. Avrami, Kinetics of phase change. I General theory, *J. Chem. Phys.* **7**, 1103 (1939).
- [28] M. Avrami, Kinetics of phase change. II Transformation time relations for random distribution of nuclei, *J. Chem. Phys.* **7**, 212 (1940).
- [29] M. Avrami, Kinetics of phase change. III Granulation, phase change and microstructure kinetics of phase change, *J. Chem. Phys.* **9**, 177 (1941).
- [30] D. B. Hayes, Wave propagation in a condensed medium with N transforming phases: Application to solid-I–solid-II–liquid bismuth, *J. Appl. Phys.* **46**, 3438 (1975).
- [31] C. N. R. Rao *et al.*, *Phase Transitions in Solids, an Approach to the Study of the Chemistry and Physics of Solids*. Advanced book program (McGraw-Hill, New York, 1978).
- [32] N. Hamaya, Y. Yamada, J. D. Axe, D. P. Belanger, and S. M. Shapiro, Neutron scattering study of the nucleation and growth process at the pressure-induced first-order phase transformation of rbi, *Phys. Rev. B* **33**, 7770 (1986).